Enhanced Geothermal Reservoir Characterization Using Wireline Distributed Acoustic Sensing

Martuganova, Evgeniia; Norden, Ben; Blöcher, Guido; Krawczyk, Charlotte M.

DOI
10.1002/9781394179275.ch21

Publication date
2024

Document Version
Final published version

Published in
Distributed Acoustic Sensing in Borehole Geophysics

21

Enhanced Geothermal Reservoir Characterization Using Wireline Distributed Acoustic Sensing

Evgeniia Martuganova[1,2], Ben Norden[2], Guido Blöcher[2], and Charlotte M. Krawczyk[2,3]

ABSTRACT

Successful across-scale reservoir characterization is a prerequisite for sustainable utilization of the subsurface. Here, we discuss aspects of distributed acoustic sensing (DAS) vertical seismic profiling (VSP) acquisition in Germany and provide an example of data integration for reservoir characterization at the geothermal research platform Groß Schönebeck, aiming to utilize Permian and Permo-Carboniferous reservoir sections at depths below 4 km. At this site, DAS VSP wireline data obtained in two boreholes were processed successfully for 3D interpretation. The data and their interpretation serve as input for a fundamental update of the structural and property characterization of the reservoir zones, relying on the integration of conventional surface 3D seismics and joint core-log analysis. The new model provides a much more detailed characterization of the target reservoirs, allowing for the first time a geological-based (facies-driven) parameterization of the subsurface, considering hydraulic and thermal properties of the reservoir-forming rocks.

21.1. INTRODUCTION

One of the European Union (EU)'s key development objectives is to become the first climate-neutral continent by 2050. Alongside various proposed actions, such as cutting greenhouse gas emissions and developing carbon capture and storage (CCS) facilities, the expansion of renewable energy sources is an essential part of the EU's decarbonization efforts (The European Commission, 2018). Among the currently available renewable resources, geothermal energy, unlike solar and wind, has the advantage of not being dependent on weather variations and does not require a large amount of land, which becomes especially important in urban areas (Roadmap for Deep Geothermal Energy for Germany, 2022). By 2050, the geothermal sector is expected to achieve 2,570 TWh (The European Commission, 2021).

Currently, Germany has in total approximately 190 geothermal installations operational for direct utilization of geothermal energy with an available geothermal capacity equal to 406.9 MWth with a geothermal heat production of 6,183.7 TJ (Weber et al., 2022). Most of the installations are realized in the shallow subsurface. In February 2023, 42 deep geothermal energy projects were in operation with a total capacity of 417 MWth (Bundesverband Geothermie, 2023). Most of the deep geothermal district heating and power plants are situated in the Molasse Basin in Southern Germany, owing to the favorable geological conditions showing high productivity and low salinity of the geothermal fluid originating from a karstic aquifer system (Figure 21.1(a)). Deep geothermal installations are more challenging to apply in the Upper Rhine Graben and the North German Basin. Here,

[1]*Department of Geoscience & Engineering, Delft University of Technology, Delft, The Netherlands*

[2]*Helmholtz Centre Potsdam, GFZ German Research Centre for Geosciences, Potsdam, Germany*

[3]*Department of Applied Geophysics, Technische Universität Berlin, Berlin, Germany*

Distributed Acoustic Sensing in Borehole Geophysics, Geophysical Monograph 289, First Edition.
Edited by Yingping Li, Robert Mellors, and Ge Zhan.

DOI: 10.1002/9781394179275.ch21

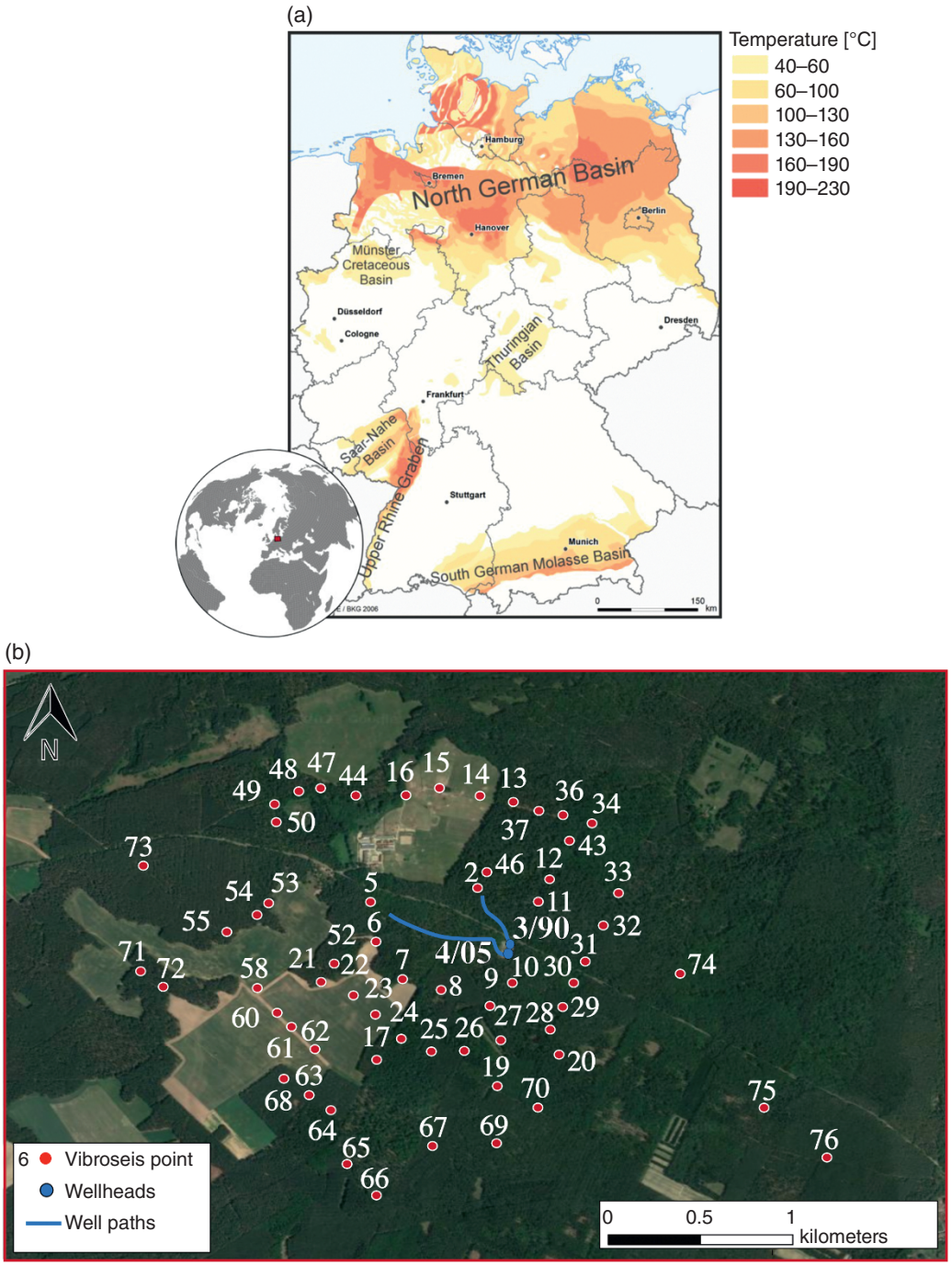

Figure 21.1 Location of the Groß Schönebeck geothermal site. (a) German hydrothermal resources regions with associated temperature ranges. Adapted from Suchi et al. (2014). (b) Base map of the Groß Schönebeck geothermal site with two boreholes (blue circles) in the center and 61 VSP source points (red dots) arranged in a spiral pattern around.

the more complex geological setting requires a customized exploration approach to account for possible risks in the geothermal exploitation of deep reservoirs. Thereby, the geothermal market in Germany has a significant potential for expansion, aiming to cover over 300 TWh/yr (Roadmap for Deep Geothermal Energy for Germany, 2022). To further stimulate the demand for geothermal energy, the Federal Ministry for Economic Affairs research funding has a significant focus on continuously developing exploration techniques, which will allow for minimizing the risk of failure to find a suitable reservoir and lower high upfront investment costs for geothermal projects (Federal Ministry for Economic Affairs and Climate Action of Germany, 2014).

The application of distributed acoustic sensing (DAS) measuring techniques to acquire seismic data reduces acquisition costs. It provides high-resolution data at considerable depths, which is especially important for deep geothermal reservoirs due to the high drilling costs. The installation of fiber-optic cables and the usage of DAS acquisition methods in Germany are quite limited and have more of a research focus. However, further technological advancement may allow the implementation of this data acquisition method into a standard geothermal exploration program.

Besides the application of DAS for deep geothermal systems, the technology is also applied in so-called aquifer thermal energy storage (ATES) systems. In total, 56% of the primary energy consumption in Germany is utilized for heating and cooling purposes (Federal Ministry for Economic Affairs and Climate Action of Germany, Berlin, Germany, 2019), whereas often, heat (or cooling) is only temporarily needed. Therefore, besides direct uses of geothermal energy, applying ATES systems in the shallow subsurface is increasingly becoming popular as seasonal energy storage for district heating or cooling. The limited deployment of such systems in Germany is caused partially due to the fear of potential interference with shallow freshwater aquifers used for drinking water supplies (Frick et al., 2022). Thus, licensing authorities and developers have shifted their focus toward deeper and saline aquifers, demanding a profound characterization of the target aquifers and their overburden. Moreover, such subsurface installations need to be close to the user. Conventional exploration using 2D and 3D geophysical surveys is limited in urban areas. In Berlin, an ongoing research project focuses on strategies for developing adjusted exploration and utilization concepts for safe, reliable, and efficient integration of ATES systems in the local distribution network.

The research project GeoFern investigates potential Mesozoic storage targets for seasonal heat storage in Berlin-Adlershof. Within this framework, a research well was drilled to study the geological sequence and its storage suitability, and an innovative seismic exploration approach using DAS technology was conducted. The latter included an acquisition using a so-called dark fiber position along a major road. Here, the data were analyzed using multichannel analysis of surface waves with the coherency-based enhancement of wavefields (Ehsaninezhad et al., 2024). In addition, vertical seismic profiling data recorded using fiber-optical cable inside a shallow borehole behind the casing and weight drop as a source are planned to be used for further investigations, such as velocity profile characterization and imaging.

The growing demand for deep geothermal energy utilization poses new challenges not only for exploration campaigns but also for monitoring geothermal sites. For instance, installing permanent monitoring systems in geothermal production wells equipped with an electrical submersible pump is technically demanding because the monitoring method should refrain from intervening with the production process. Equipment of the borehole with fiber-optic cable can provide a solution for permanent monitoring.

The first attempt of using a fiber-optic monitoring system along the whole length of the production well was tested in the Molasse at the geothermal site Schäftlarnstraße in Munich, Germany. The production borehole was equipped with a fiber-optical cable, installed inside the well using the mounting method on the rigid pump sucker rod, which acts as a centralizer and helps to guide flexible cable and prevent it from coiling, which is especially beneficial in deviated boreholes (Lipus et al., 2022). The installed cable comprises two DAS fibers, two distributed temperature sensing fibers, and a single fiber for a down-hole fiber-optic pressure/temperature gauge that was attached to the sucker rods, reaching the measured depth of 3691 m (Schölderle et al., 2021). The data collected in a post-drilling period (during borehole tests and geothermal operational activities) were used to characterize hydraulically active zones in the karstic Upper Jurassic reservoir (Schölderle et al., 2021). The DAS data provided confirmation that the temperature drop that occurred during the injection of cold water was responsible for the contraction/expansion moves of the sucker rod/fiber cable setup (Lipus et al., 2022). In addition, the data recorded during the beginning of the injection test agree well with the injection profile data (Schölderle et al., 2021). Overall, the fiber-optical sensing setup performed well during the tests, proving the possibility of further investigation to detect microseismicity events and provide information on well integrity.

In the case of repurposing accessible drilled (legacy) boreholes for geothermal characterization of the subsurface, the application of the wireline DAS technique can provide a convenient and cost-efficient way to acquire additional data necessary for successful exploration. In the following, we will focus on this type of DAS application based on the Groß Schönebeck case study.

21.2. THE GEOTHERMAL RESEARCH PLATFORM GROß SCHÖNEBECK

The in situ geothermal laboratory Groß Schönebeck aims to develop and test concepts for heat extraction from deep, naturally low-permeable rock units below the Permian Zechstein salt. The site is located approximately 50 km NE of Berlin in the natural reserve Schorfheide, Brandenburg, Germany, at the southern margin of the North German Basin (NGB) (Figure 21.1(a)). Two research wells encountered sedimentary Permian Rotliegend and Permo-Carboniferous volcanic rocks, providing

access to water-bearing horizons at depths between 3.9 and 4.3 km at temperatures of 150 °C but with low productivity (Zimmermann et al., 2010). A viable exploitation of the deeply stored geothermal energy might be possible by applying engineering measures to allow sufficient heat extraction. At the Groß Schönebeck site, research is focusing on possibilities of reservoir stimulation to support the further development of strategies for the successful implementation of so-called enhanced geothermal systems (EGSs; e.g., Tester et al. (2006); Olasolo et al. (2016)). Altogether, seven stimulation treatments were carried out between 2002 and 2007 in different depth intervals (Blöcher et al., 2016).

However, successful geothermal utilization of the target horizons has not been possible so far. One of the boreholes of the research platform, the E GrSk 3/90 well, was initially drilled for gas exploration and reopened and deepened for geothermal production in 2001. The second well, the Gt GrSk 4/05 borehole, was drilled in 2006 for geothermal production from a geothermal doublet. After first promising stimulation treatments showing an increase in productivity by more than a factor of 4 (Zimmermann et al., 2011), the further site development resulted in shutdown periods for the geothermal production. From 2011 to 2013, in total, 139 hydraulic experiments were conducted at the site (Blöcher et al., 2016), trying to establish an enduring geothermal heat production. However, the experiments document a sharp reduction of productivity, possibly caused by the accumulation of minerals and copper precipitation (scales) clogging the production well, forming a wellbore skin (Regenspurg et al., 2015). Other reasons for the productivity decrease were discussed by Blöcher et al. (2016), as a single process will not account for all well-test results (e.g., two-phase flow due, free gas, and possible compartmentalization of the target horizons by fault zones).

The influence of fault zones on the hydraulic behavior of the reservoir has been investigated in several numerical studies. A direct pressure response between the two wells could be traced back to a poroelastic behavior (Jacquey et al., 2016), and microseismic events measured during a stimulation treatment were outside the previously interpreted fault zones (Blöcher et al., 2018). The conclusion can be drawn here that the previously interpreted fault zones are not hydraulically active or even nonexistent.

To allow well-founded further site development, further geophysical exploration campaigns were initiated in 2017, covering a 3D surface seismic survey and a DAS vertical seismic profiling (VSP) seismic surveying. The resulting data form the basis for the presented case study.

21.3. DATA INTEGRATION FOR GEOLOGICAL AND PETROPHYSICAL CHARACTERIZATION

21.3.1. 3D Seismic and Wireline DAS Acquisition Campaign

A 3D surface seismic campaign was conducted in February–March 2017 (Krawczyk et al., 2019; Stiller et al., 2018). Until then, the deeper geology of the site was interpreted from sparsely distributed legacy 2D seismic lines from former hydrocarbon exploration. The 3D data should therefore deepen the structural understanding of the reservoir section, locate possible faults and fractures, and help to understand the general geological setting better. The 3D surface seismic survey covers an area of 8 km by 8 km, focusing on target reservoir depth from 4 to 4.3 km. The reservoir section is overlain by more than 1 km of thick Zechstein salt, significantly reducing the frequency range and, therefore, the resolution at the target depths, and providing a challenging geological setup for the seismic campaign. The 3D seismics allows for the first time a consistent geological interpretation and model parameterization of the site (Norden et al., 2023).

The 3D surface seismic campaign was accompanied by a VSP experiment using wireline DAS to bridge resolution gaps from the borehole to the field scale. The VSP method benefits from the shorter travel times and, therefore, can provide higher-resolution data. Thus, to improve the resolution of the seismic imaging results around the boreholes, a complementary VSP experiment was conducted before the main 3D surface seismic campaign. Furthermore, the application of fiber-optical cable for seismic data measurements enabled data acquisition at elevated temperatures of 150° during four acquisition days (Henninges et al., 2021). The temperature at the Groß Schönebeck geothermal site is within the temperature limit of geophone's applications, and moreover, geophones can withstand these temperatures only for a limited amount of time (Kästner et al., 2020). Thus, wireline DAS VSP allowed for significant time and cost savings for the survey that was conducted.

The dataset was recorded in February 2017 within four acquisition days: one day of start-up testing and three acquisition days. VSP data were acquired from two 4.3-km-deep wells: E GrSk 3/90 (maximum inclination 7.2°) and Gt GrSk 4/05 (maximum inclination 49°), using a hDVS (Heterodyne Distributed Vibration Sensing, Schlumberger) interrogator system connected to a wireline cable. The spatial spacing along the cable was processed to 5 m. A summary of receiver parameters is presented in Table 21.1.

Table 21.1 Receiver acquisition parameters.

Parameter	E GrSk 3/90	Gt GrSk 4/05
Interrogator type	Schlumberger hDVS unit	Schlumberger hDVS unit
Type of wireline cable	GFZ–Rochester (Henninges et al., 2011)	Schlumberger–NOVA-F
Type of fiber	Single-mode	Single-mode
Slack on the cable	1 m	1 m
Recorded type of data	Strain	Strain
Depth interval receiver channels	Ground level – 4,251 m MD	Ground level – 3,716 m MD
Recorded number of vibroseis points	61	18
Spatial sampling along borehole	5 m	5 m
Gauge length	40 m	20 m
Sampling interval	2 ms	2 ms
Trace length (after correlation)	4 s	4 s
Polarity convention	European/EAGE normal	European/EAGE normal

Table 21.2 Source acquisition parameters.

Parameter	Value
Seismic source	Four vibrator trucks: Mertz M12 Hemi 48, peak force 200 kN (45,100 lbf) each
Number of source points	61
Offset	188–2,036 m
Sweep (near offsets)	10–112 Hz, linear up, 36 s, 360 ms taper
Sweep (far offsets)	10–96 Hz, linear up, 36 s, 360 ms taper
Average vertical stacking fold	16 per source location

The 61 vibroseis points (VPs) were positioned in a spiral configuration with offsets varying between 188 and 2,036 m (Figure 21.1(b)). Source acquisition parameters are summarized in Table 21.2. In borehole E GrSk 3/90, a total of 61 VPs were recorded, with a maximum depth of 4,251 m measured depth (MD). Due to cable failure, the number of VPs and maximum measured depth recorded using the cable placed in Gt GrSk 4/05 is limited to 18 VPs and 3,716 m MD, respectively. More information and possible explanations of the incident can be found in Henninges et al. (2021).

21.3.2. Coupling Noise in Wireline DAS VSP Measurements

In wireline installations, the measuring fiber-optical cable is freely suspended inside the borehole. This allows for cost-effective data acquisition in already-drilled boreholes, but it comes at the expense of reduced data quality due to coupling conditions that are difficult to control and are therefore suboptimal. Wireline DAS data are often affected by specific coupling noise, which we observed in our data. Raw strain data have a pronounced pattern of high-amplitude areas (Figure 21.2(a)), which, after correlation with the pilot sweep, creates a distinct zigzag pattern (Figure 21.2(b)). This characteristic noise is typical for wireline DAS recordings and was described in the literature by Hartog et al. (2014), Dean et al. (2015), Yu et al. (2016), and Martuganova et al. (2021).

In Martuganova et al. (2021), the authors propose that this noise represents a standing wave phenomenon generated on poorly coupled depth intervals of the fiber-optical cable (Figure 21.3(a)) by a vibroseis signal. A classical displacement formula can be utilized to compute a synthetic model for the first four harmonics for fixed-end string case and thus clarify the nature of zigzag patterns found in the data:

$$U = 2A \sin \frac{n\pi x}{L} \cos \omega t, \tag{21.1}$$

where A is the displacement amplitude, n is an integer mode number, x is a spatial coordinate, L is the length of the string, ω is an angular frequency, and t is time.

Figure 21.3(b) shows that the displacement for fixed cable ends is theoretically described for the fundamental mode and three overtones. The output of the hDVS interrogator unit is strain. To convert data from displacement to strain, the data were differentiated over spatial coordinates (Figure 21.3(c)). The positions of nodes and antinodes will be interchanged due to differentiation, and therefore, the standing wave for closed-end strain recording will look like displacement for the free-ends case. In the case of an odd number of the harmonic, the strain at the ends of the string is out of phase, and for an even number, it is in phase (Figure 21.3(c)). The transition of the mode from odd to even will change the phase of the one end of the string. This disproportion in phases at the string ends will create the zigzag pattern after correlation with different up and down velocities (Figure 21.3(d)).

21.3.3. 3D DAS VSP Data Processing

The processing flow for the 3D DAS VSP dataset consists of typical elements for 3D VSP data processing (Table 21.3), with necessary adjustments for the specifics of the Groß Schönebeck survey, such as the elimination of the coupling noise described earlier. We applied the

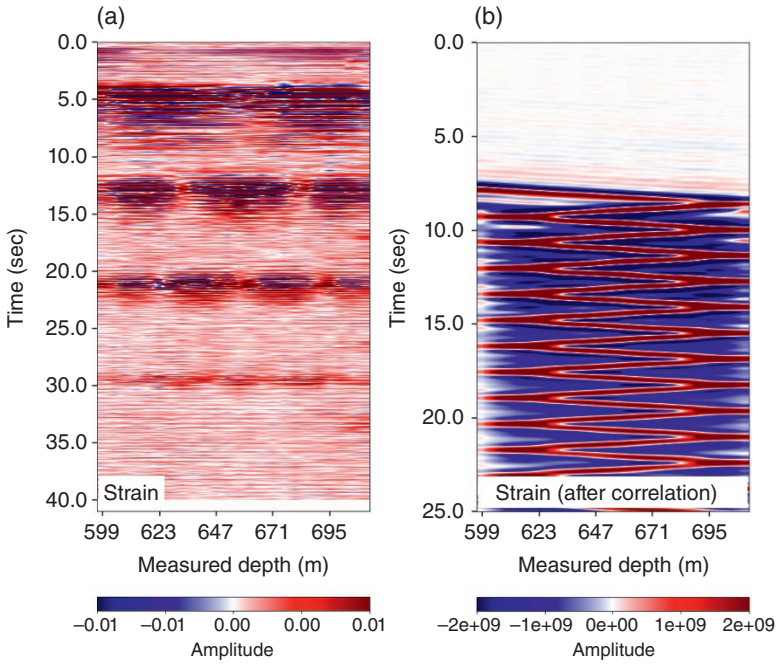

Figure 21.2 (a) An example of field strain data recording for the depth interval 597–711 m. (b) Field strain data recording after correlation.

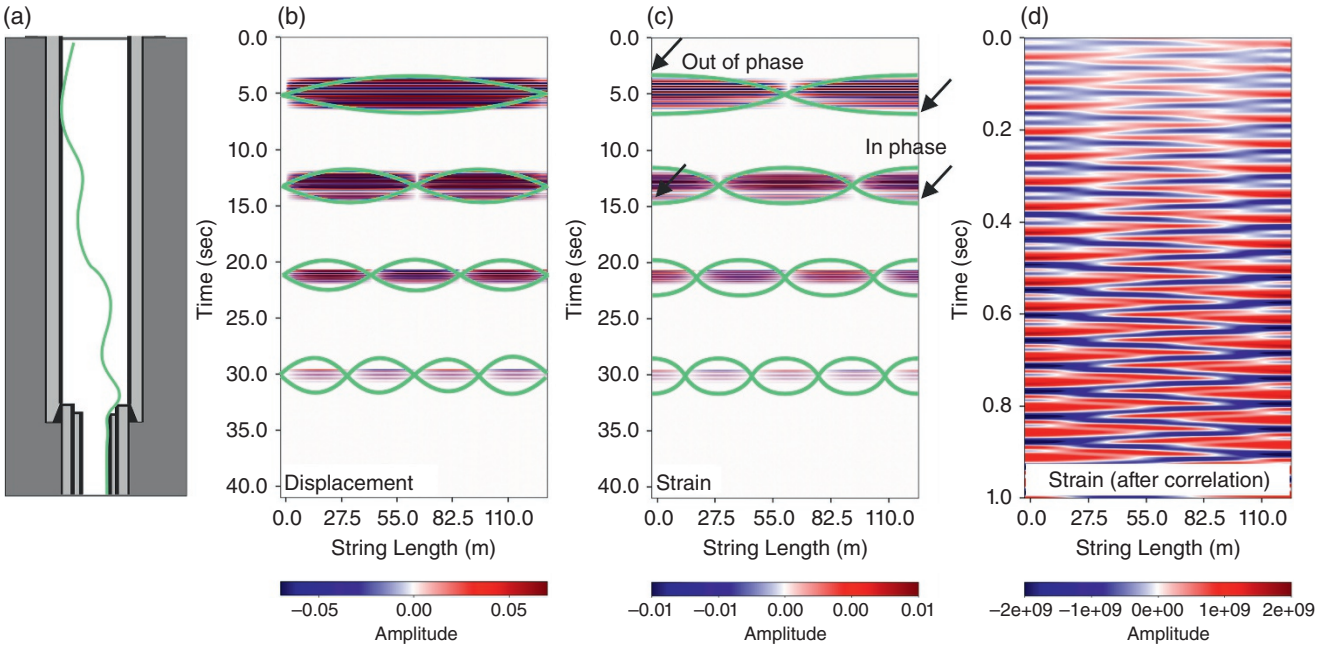

Figure 21.3 An explanation of the noise pattern generation during the wireline survey. (a) A sketch representing wireline cable positioning inside the casing. (b) Modeled displacement for fixed-end cable vibrations for one the main tone and three overtones; the bold green line shows theoretical cable movement for the corresponding frequency mode. (c) Modeled strain; the bold green line shows theoretical cable movement for the corresponding frequency mode. (d) Modeled strain after correlation with a sweep signal.

matching pursuit decomposition (MPD) method (Martuganova et al., 2021) first to decompose a raw stacked seismic trace (Figure 21.4(a)) into elementary Gabor waveforms (an example of elementary Gabor functions is shown in Figure 21.4(b)). Through detailed analysis of elementary functions parameters used for signal decomposition, such as frequency, phase, amplitude, and temporal position, the part of the signal associated

Table 21.3 3D DAS VSP data processing flow for wells E GrSk 3/90 and Gt GrSk 4/05.

Processing step	Description and parameters
Geometry input	Source and receiver coordinates, depths
Trimmed mean stack	Suppression of impulsive noise
Ringing noise suppression	MPD with Gabor atoms
Correlation with pilot sweep	10–112 Hz, 10–96 Hz, 36 s, 360 ms taper
Conversion to strain rate	Time derivative
First-arrival time picking	The peak of the direct downgoing P-wave
Amplitude corrections	Spherical divergence compensation ($t^{1.5}$) and lateral equalization
Coherency enhancement	Moderate wavefield sharpening by tau-p method
Velocity model building	Migration velocities from 3D surface seismics and sonic log from E GrSk 3/90 as initial velocity model, checked and optimized by ray tracing
Ray tracing	Mapping of the reflectivity for all source receiver pairs
Wavefield separation	Subtraction of downgoing P-wave field (median filter) by a nine-trace median operator
Deterministic deconvolution	Waveshaping zero-phasing of the upgoing wavefield, removal of multiples
Polarity reversal	180° phase shift to match polarity convention of conventional geophone data
3D imaging	3D Kirchhoff migration with restricted aperture of 12°

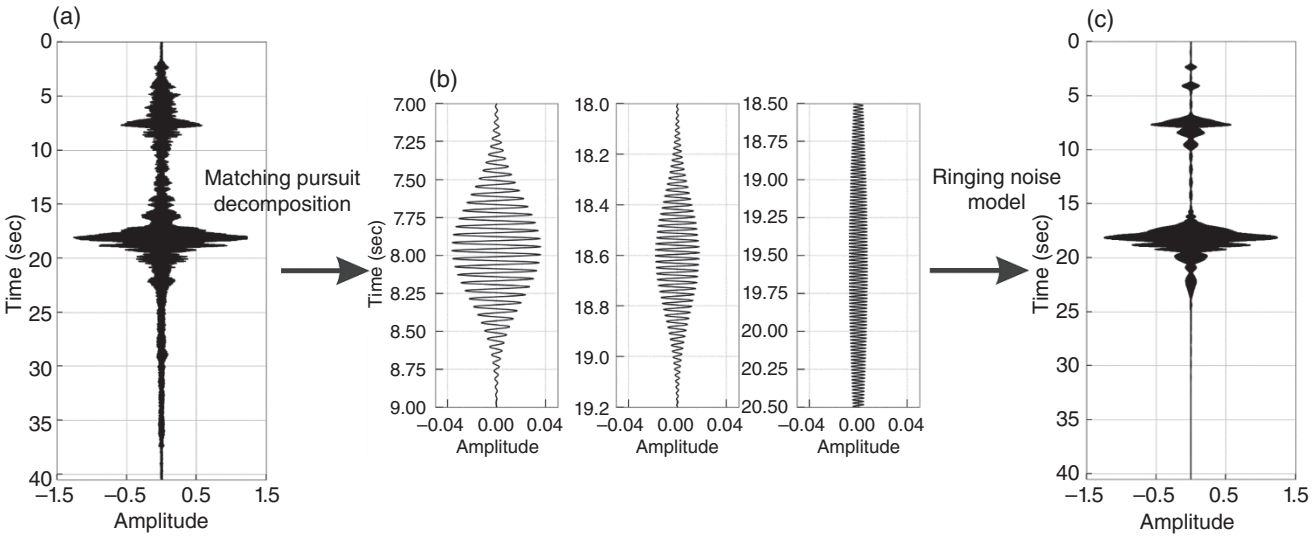

Figure 21.4 An explanation of the matching pursuit algorithm. (a) Raw stacked strain data before the decomposition process. (b) Examples of Gabor elementary functions used to fit the original seismic trace. (c) A coupling noise model, which was generated using selected Gabor atoms.

with cable slapping and ringing was identified and used to create a model of the noise (Figure 21.4(c)). Compared to the original data with standard preprocessing applied (stacking, correlation with pilot sweep, and differentiation in time domain) shown in Figure 21.5(a), we observe that the amplitude and phase of the coupling noise (Figure 21.5(b)) is accurately reconstructed. The created noise model was subtracted from the original raw strain data, and the same preprocessing flow was applied to the seismic section shown in Figure 21.5(c).

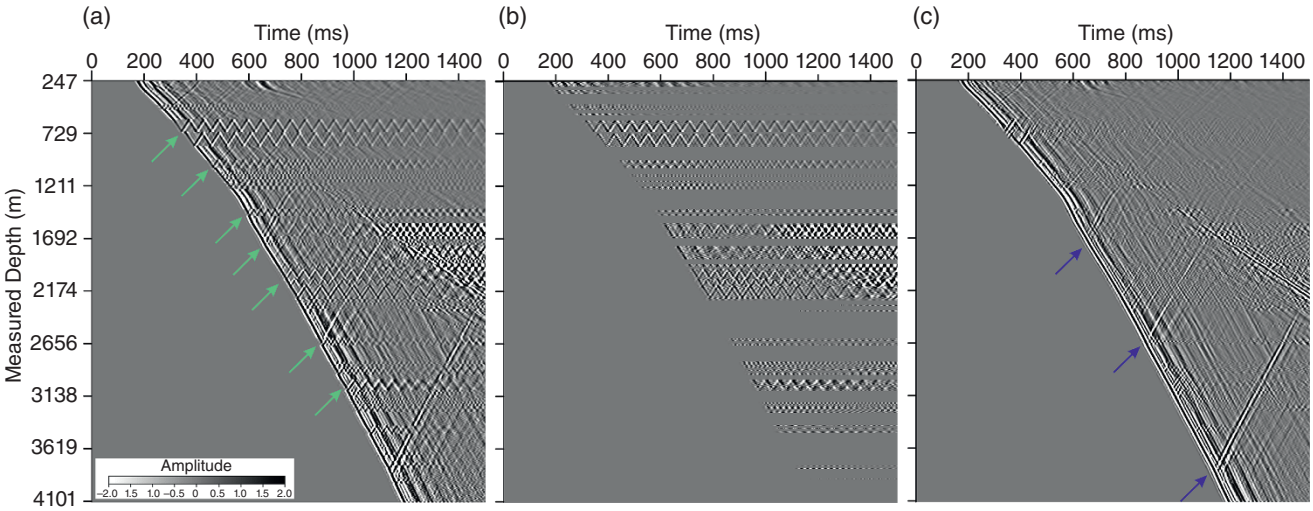

Figure 21.5 Common-source gather acquired at source position 10 (Figure 21.1(b)). (a) Before the denoising; (b) the coupling noise model, created using MPD decomposition method; (c) common-shot gather after the noise model was subtracted. Light green arrows in (a) highlight depth intervals affected by the coupling noise; blue arrows in (c) show improved traceability of the reflections in VSP data.

After vertical trimmed mean stacking and removal of the typical wireline acquisition coupling noise, the VSP data preparation consisted of geometry input, correlation with the pilot sweep, and subsequent differentiation in the time domain to convert data into strain rate and achieve acceleration-like characteristics. Further processing included first-arrival picking, spherical divergence, lateral amplitude equalizations, and moderate wavefield sharpening using the tau-p method. To obtain a 3D seismic image in the depth domain, first we constructed a preliminary velocity model using velocities from 3D surface seismics and sonic log from well E GrSk 3/90, which was checked and adjusted using the ray-tracing method. The following processing step included wavefield separation by subtracting the downgoing wavefield using a median filter, followed by deterministic deconvolution. The 3D DAS VSP image was computed using the commercial algorithm (VSProwessX) 3D Kirchhoff migration algorithm with a restricted aperture of 12°. A more detailed description of 3D DAS VSP data processing can be found in Martuganova et al. (2022a).

21.3.4. Geological Modeling and Petrophysical Model Parameterization

The geological and petrophysical characterization could rely on different data types ranging from the laboratory scale to the borehole and across borehole scales, including the reservoir level. Information on the lithology and stratigraphy and the overall geological setting is provided by the Groß Schönebeck site's boreholes and neighboring wells. Petrophysical data are accessible from the E GrSk 3/90 borehole. Starting from a seismic-well tie interpretation (Krawczyk et al., 2019), seismic horizons were mapped and lithologically interpreted (Norden et al., 2023). The well control allows linking the seismically mapped Rotliegend succession to lithotypes and sedimentary facies patterns. To better constrain the internal structure pattern of the sedimentary Rotliegend, a wavelet transform-based seismic facies classification using neural network clustering (Bauer et al., 2020) was applied to resolve information stored in the signal attributes calculated along the target horizon. Based on the constructed structural model, a reservoir model was set up for further site development (Norden et al., 2023). The model comprises the Permo-Carboniferous volcanic rock section and the sedimentary Rotliegend. In the first step, the structural units and facies types were modeled using a stochastic approach. Then, the respective units were parameterized with petrophysical properties (e.g., total and effective porosity, permeability, density, bulk thermal properties; see also Figure 21.6), considering each facies type with its respective property distribution characteristics. The Groß Schönebeck dataset provided by Norden et al. (2022) forms the basis for this second step in model building. It comprises an extensive evaluation of legacy data and newly acquired measurements and interpretations for core-log integration.

For the facies-dependent petrophysical parameterization, the total porosity distribution as the most robust allocatable property was modeled based on the respective geostatistical input derived from the core-log integration. For the sedimentary Rotliegend, the Elbe reservoir sandstone's porosity distribution was modeled using the

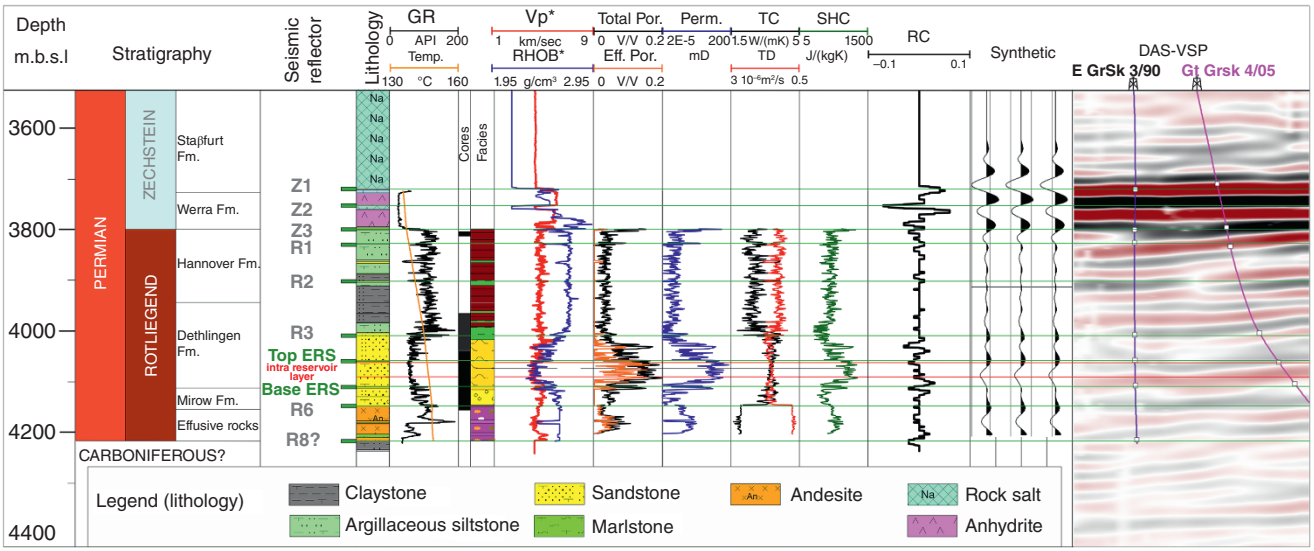

Figure 21.6 DAS VSP seismic cross-section through the boreholes plotted together with well-log related data from the E GrSk 3/90 borehole (GR, gamma ray; Vp, sonic velocity; RHOB, bulk density), petrophysical properties from core-log integration (Total Por., total porosity; Eff. Por., effective porosity; Perm., permeability; TC, thermal conductivity; TD, thermal diffusivity; SHC, specific heat capacity), lithology, stratigraphy, reflector coefficient (RC), and synthetics.

seismic facies analysis of Bauer et al. (2020) and the observations of the DAS VSP analysis of Martuganova et al. (2022a) as trend data. For the sedimentary units, effective porosity was modeled in relation to total porosity using collocated co-kriging and bulk density of the rocks, and the shale content was assigned to the grid cells. They were simulated based on the distribution of total porosity (for bulk density) and effective porosity (for the shale content from GR) using the determined geostatistical input parameter. Permeability was calculated on total porosity. In situ thermal conductivity and diffusivity were estimated using the density and shale content distributions based on formulas provided by Fuchs et al. (2015) for well-log interpretation. The specific heat capacity was calculated from the evaluated distributions of thermal conductivity, thermal diffusivity, and density. The approach for the parameterization of the Permo-Carboniferous volcanic rocks was similar. Here, density, effective porosity of interconnected pores, and permeability were simulated using the geostatistical input data and the collocated co-kriging with the total porosity distribution. For details, see Norden et al. (2022) and Norden et al. (2023).

21.4. RESULTS

The geothermal research platform Groß Schönebeck has focused on two possible targets for geothermal exploration so far: the low-porous Permo-Carboniferous volcanic rocks and the sandstones of the Lower Elbe Subgroup (Dethlingen formation). The geophysical surveys performed at the site should help to understand the reservoir setting and clarify possible structural obstacles that may hinder geothermal utilization. In the following subsections, we characterize these subsalt geothermal targets based on the 3D surface and the 3D DAS VSP seismic cubes, available core information, well logs, laboratory data, and the results of the stochastically parameterized facies-dependent petrophysical property distributions.

21.4.1. Permo-Carboniferous Volcanic Rocks

The top of Permo-Carboniferous volcanic rocks was encountered in the E GrSk 3/90 borehole at a depth of 4216 m TVDSS (Reflector R8, Figure 21.6). This reflector is traceable within the 3D surface and the 3D DAS VSP seismic data. In the 3D DAS VSP cube, this boundary is characterized by a change of the seismic reflection pattern: from a more or less horizontal to a more inclined layering (red line, Figure 21.7), with numerous pinch-outs below. Martuganova et al. (2022a) refer to this feature as the Lower Rotliegend unconformity. According to Guterch et al. (2010), Lower Rotliegend has significant time gaps in sedimentation; therefore, the mapped unconformity horizon could indicate a difference in layering caused by erosion.

Volcanic rock cores from the E GrSk 3/90 borehole are characterized by several layered lava beds and tuffs with a single bed thickness of 1 to over 3 m; the mean flow

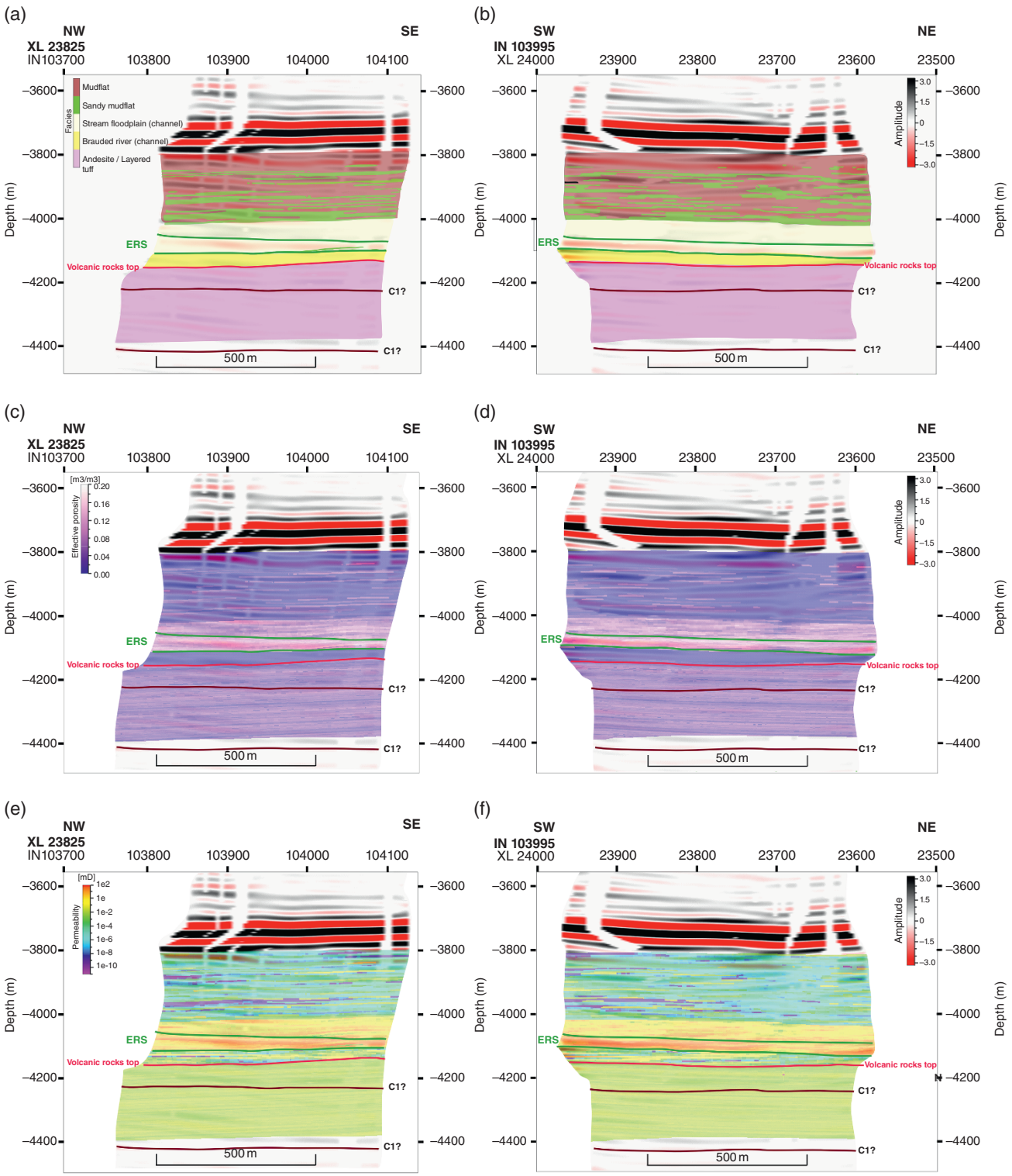

Figure 21.7 Seismic lines extracted from the 3D DAS VSP cube with facies (a, b) and petrophysical parameterization (c–f). Green lines show the borders of the Elbe basis reservoir sandstone layer, red lines show the top of the volcanic rocks, and burgundy lines annotated C1? highlight possible interpretations for the base of Carboniferous.

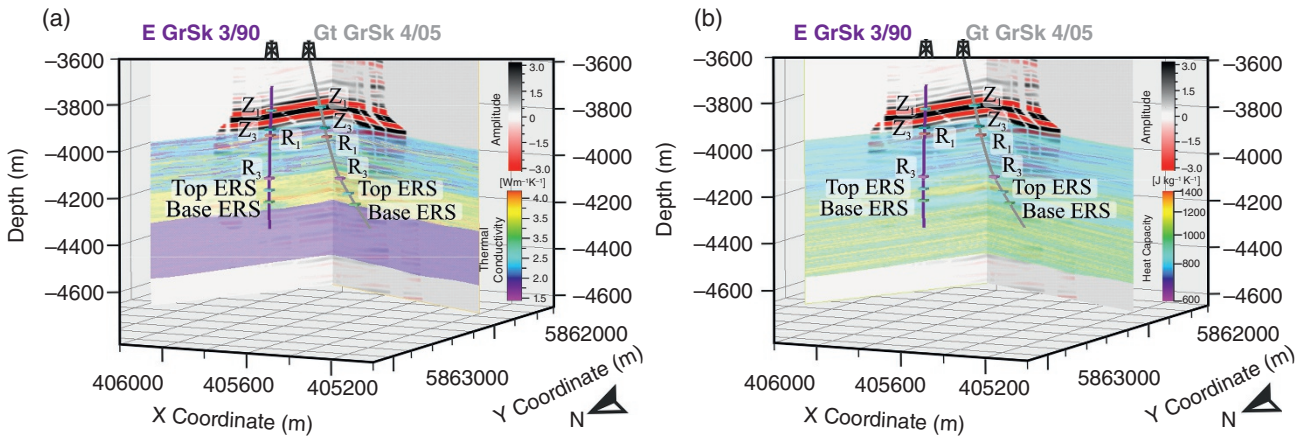

Figure 21.8 The 3D visualization of the thermophysical properties illustrates the expected variability of property distribution in the vicinity of the boreholes. 3D DAS VSP cube overlaid by (a) thermal conductivity and (b) heat capacity.

direction of the andesitic lava indicated from image logs show north to north–northwest direction (Norden et al., 2023). Thus, the internal structure of the volcanic sequence is below seismic resolution. Here, the image log of the E GrSk 3/90 provides the main input for the geological model. Based on gamma-ray (GR) and sonic logs and to some extent on laboratory measurements on cores (density, porosity, permeability, thermal conductivity), the modeled volcanic sequence was parameterized (Figures 21.7 and 21.8). Effective porosity shows mean values of about 2% and 4% for tuffitic and andesitic layers and mean matrix permeability of 9.9 E–18 m^2. Mean values of the volcanic sequence for the thermal conductivity amount to 1.9 $Wm^{-1}K^{-1}$ (Figure 21.8(a)), the mean thermal diffusivity to 0.69 $10^{-6}/m^2/s^{-1}$, and the specific heat capacity to 1025 $Jkg^{-1}K^{-1}$(Figure 21.8(b)).

Unfortunately, the top of the sedimentary Carboniferous underlying the volcanic succession could not be resolved with certainty from either seismic or borehole data (Norden et al., 2023). The thickness of the volcanic may amount to a 70 m or about 200 m thick sequence (burgundy lines with annotations C1? in Figure 21.7). Therefore, because we have only limited data from one borehole, the shown property distribution within the volcanic sequence represents a first-order estimation. This will be used to design hydraulic stimulations and estimate the geothermal potential of this sequence.

21.4.2. Sedimentary Rotliegend (Including Elbe Reservoir Sandstone)

Sedimentary Rotliegend succession is located in the depth interval between 3,800 and 4,216 m comprising Mirow, Dethlingen, and Hannover Formations (Figure 21.6). In this lithostratigraphic unit, four different sedimentary facies types were considered in the modeling: the mudflat playa, the sandy mudflat, the ephemeral stream floodplain, and the braided river facies (Figures 21.7(a), (b)). The latter facies type dominates the Mirow Formation, overlaying the volcanic succession. According to Holl et al. (2005), most of the coarse-grained bed-load-dominated and conglomeratic deposits of this formation are interpreted as multistoried channel sediments of a braided plain fluvial system with a paleocurrent direction toward NNE. The conglomerates, consisting of cemented volcanic rocks, show a porosity similar to that of volcanic rocks and low matrix permeability (Norden et al., 2023). However, the mean thermal conductivity of this unit is higher than that of the volcanic rocks and amounts to about 3.7 $Wm^{-1}K^{-1}$ (Figure 21.8(a)).

According to the core information from the E GrSk 3/90 and Gt GrSk 4/05 wells, a more porous sandstone is present in the Dethlingen Formation above the Mirow Formation (Bauer et al., 2020; Norden et al., 2023). This so-called Elbe reservoir sandstone (ERS) was encountered in the depth interval 4,060–4,100 m at the E GrSk 3/90 borehole. On well logs, this interval is observed as a low P-wave velocity zone due to the increased porosity of this section (Figure 21.6). The ERS unit in the geological model is based on the depth of the mapped horizons of the top and base ERS from the 3D surface seismic cube. These horizons were correlated to the drilled well tops and adjusted considering the information from the thickness distribution pattern extracted from the wavelet analysis, providing trend information on possible thickness changes below seismic resolution. In the vicinity of the boreholes, the picked horizons from the 3D DAS VSP cube were integrated into the structural model (Norden et al., 2023). In Figure 21.7, the borders of this unit are shown using green lines. The ERS represents sediments

that were initially formed in an aeolian environment and later redeposited by fluvial processes of the ephemeral stream floodplain. The rocks of these facies show the most robust porosity–permeability relationship because they represent quartz-dominated sandstones with only minor clay content (Norden et al., 2023). However, the derived in situ fluid permeability for the ERS unit ranges from less than 1 mD (1 E–15 m^2) to more than 100 mD (1 E–13 m^2) with an overall geometric mean of only some mD (Figure 21.7(e), (f)). The mean thermal conductivity amounts to about 3.6 $Wm^{-1}K^{-1}$ (Figure 21.8(b)). The joint interpretation of the geophysical data did not provide evidence of structural compartmentalization of the reservoir; the range of variation is covered by the expected geological heterogeneity (Norden et al., 2023).

The sediments of the Upper Dethlingen and Hannover Formations are dominated by rocks of the mudflat and sandy mudflat environment. They show a more complex facies distribution pattern. Effective porosities are low (in the order of 0–3% (Figure 21.7(c), (d)), and due to the higher clay content compared to the ERS, the thermal conductivity of these formations is lower and in the order of 3.2 $Wm^{-1}K^{-1}$ for the sandy mudflat and 2.2 $Wm^{-1}K^{-1}$ for the mudflat facies (Figure 21.8(a)).

21.5. DISCUSSION

Although the seismic data could not provide evidence for structural boundaries (block or fault compartments), the facies and parameter modeling results show that the ERS slightly reduced reservoir properties along the Gt GrSk 4/05 borehole. They could reflect the natural heterogeneity of the reservoir. Based on the new reservoir characterization, detailed information on the principle geometry in three dimensions is given. Former models did apply a simple layer-cake characterization approach without consideration of lateral variability. The more realistic characterization of the presented model allows better planning of future measures. For example, future studies can investigate, in detail, how the natural heterogeneity will influence the long-term behavior of the reservoir.

As stated in Norden et al. (2023), a further enhancement of the presented model parameterization could be achieved by inversion of the seismic data to better guide the distribution of petrophysical parameters. The inversion will also be limited by the scale and resolution of the geophysical (seismic) data. In complex geological environments and cases when understanding heterogeneous reservoir sections is crucial for further geothermal development, VSP and DAS VSP surveys, in particular, can help significantly improve the understanding of the subsurface because of the broader frequency range and dense depth coverage. In Groß Schönebeck case study, the 3D DAS VSP cube has better resolution (vertical resolution up to 16 m (Martuganova et al., 2022a)) than 3D surface seismics; therefore, it will be beneficial to use it as an input for the inversion and as a result resolve a detailed geological facies pattern and the accompanying petrophysical properties on a finer scale.

In recent years, after the wireline 3D DAS VSP measuring campaign conducted at Groß Schönebeck in 2017, DAS interrogators have evolved dramatically. The first generation of DAS measuring units mainly utilized coherent light sources (Lindsey et al., 2020). Their pulse length restricts their spatial resolution, and their energy limits the dynamic range of the measurement. Most recent advancements in DAS data measurements, such as the usage of engineered fibers (Sun et al., 2022), multiple stable lasers, and the chirped compression technique (Waagaard et al., 2021), allow interrogating much longer fibers with significantly reduced measurement noise. Thus, acquiring another dataset with the newer-generation interrogator unit and installing engineered fibers will improve the signal-to-noise ratio, which can further enhance the resolution of 3D DAS VSP data and extract even smaller-scale geological details from the reservoir section.

The future perspective of the in situ laboratory of Groß Schönebeck envisages heat supply in rural regions. In contrast to the previous usage concept, which focused on heat and electricity, geological units with lower temperatures can be developed here. It is, therefore, also possible to drill into the shallower Mesozoic units of the Muschelkalk (shell limestone) and Buntsandstein formations. Furthermore, the EGS development of the Rotliegend (Permian) can be refrained from, and hydrothermal development of the previously mentioned units can take place. The focus is not on reusing the existing wells but rather on drilling a new doublet system to provide the heat demanded by the surrounding villages.

21.6. CONCLUDING REMARKS

This chapter integrates and summarizes the available geophysical and geological data for the geothermal in situ research platform Groß Schönebeck. A more accurate understanding of the Rotliegend reservoir was achieved by incorporating the existing reconnaissance data with the interpretations made using new 3D seismic survey, DAS VSP data, and borehole data. The created reservoir model allows an understanding of the site on various scales, permitting more realistic planning for further development of the geothermal site. The successful 3D DAS VSP application at the Groß Schönebeck may have a critical impact on the advancement and implementation of modern and effective geothermal exploration practices in the NGB and areas with similar geological settings,

taking advantage of existing (reconnaissance) boreholes for DAS VSP wireline acquisition.

ACKNOWLEDGMENTS

Funding for the present work was provided by the German Federal Ministry of Economic Affairs and Energy (grant no. 0324065) as well as the European Commission Horizon 2020 Framework Programme (DESTRESS (grant no. 691728) and EPOS IP (grant no. 676564)).

AVAILABILITY STATEMENT

3D DAS VSP data used for this study are published at GFZ Data Services (Martuganova et al., 2022b) and are accessible at https://doi.org/10.5880/GFZ.4.8.2022.014. The parameterized reservoir model, main geological horizons, core, and well-log data are also available via the GFZ repository, https://doi.org/10.5880/GFZ.4.8.2022.013 (Norden et al., 2022). The 3D surface seismic datasets are available on request. No new data were generated, analyzed, or presented in this chapter.

REFERENCES

Bauer, K., Norden, B., Ivanova, A., Stiller, M., & Krawczyk, C. M. (2020). Wavelet transform-based seismic facies classification and modelling: application to a geothermal target horizon in the NE German Basin. *Geophysical Prospecting*, *68* (2), 466–482. Retrieved from https://onlinelibrary.wiley.com/doi/abs/10.1111/1365-2478.12853

Blöcher, G., Cacace, M., Jacquey, A. B., Zang, A., Heidbach, O., Hofmann, H., et al. (2018). Evaluating micro-seismic events triggered by reservoir operations at the geothermal site of Groß Schönebeck (Germany). *Rock Mechanics and Rock Engineering*, *51*(10), 3265–3279. doi:10.1007/s00603-018-1521-2

Blöcher, G., Reinsch, T., Henninges, J., Milsch, H., Regenspurg, S., Kummerow, J., et al. (2016). Hydraulic history and current state of the deep geothermal reservoir Groß Schönebeck. *Geothermics*, *63*, 27–43. doi:10.1016/j.geothermics.2015.07.008

Bundesverband Geothermie. (2023). Tiefe Geothermie in Deutschland 2023/24. Retrieved from https://www.geothermie.de/bibliothek/downloads.html

Dean, T., Constantinou, A., Cuny, T., Frignet, B., Hartog, A., Kimura, T., et al. (2015). *Vertical seismic profiles: now just another log?* Paper presented at the 85th SEG Annual Meeting. Expanded Abstracts, 5544–5548. doi:10.1190/segam2015-5804007.1

Ehsaninezhad, L., Wollin, C., Rodríguez Tribaldos, V., Schwarz, B., & Krawczyk, C. M. (2024). Urban subsurface exploration improved by denoising of virtual shot gathers from distributed acoustic sensing ambient noise. *Geophysical Journal International*, *237*(3), 1751–1764. doi:10.1093/gji/ggae134

The European Commission. (2018). *A european strategic long-term vision for a prosperous, modern, competitive and climate neutral economy*. Brussels (Belgium): Publications Office of the European Union. Retrieved from https://eur-lex.europa.eu/legal-content/EN/TXT/?uri=CELEX:52018DC0773

The European Commission. (2021). *Report from the commission to the European Parliament and the Council. Progress on competitiveness of clean energy technologies* (part 4/5). Brussels (Belgium): Publications Office of the European Union.

Federal Ministry for Economic Affairs and Climate Action of Germany. (2014). *Bekanntmachung Forschungsförderung im 6. Energieforschungsprogramm "Forschung für eine umweltschonende, zuverlässige und bezahlbare Energieversorgung"*. Retrieved from https://www.bmwk.de/Redaktion/EN/Artikel/Energy/research-priorities-deep-geothermal-energy.html

Federal Ministry for Economic Affairs and Climate Action of Germany, Berlin, Germany. (2019). *Energiedaten: Bundesministerium für Wirtschaft und Klimaschutz der Bundesrepublik Deutschland (BMWi)*. Retrieved from https://www.bmwk.de/Redaktion/EN/Artikel/Energy/research-priorities-deep-geothermal-energy.html

Frick, M., Kranz, S., Norden, B., Bruhn, D., & Fuchs, S. (2022). Geothermal resources and ATES potential of Mesozoic Reservoirs in the North German basin. *Energies*, *15* (6). Retrieved from https://www.mdpi.com/1996-1073/15/6/1980

Fuchs, S., Balling, N., & Förster, A. (2015). Calculation of thermal conductivity, thermal diffusivity and specific heat capacity of sedimentary rocks using petrophysical well logs. *Geophysical Journal International*, *203*(3), 1977–2000. doi:10.1093/gji/ggv403

Guterch, A., Wybraniec, S., Grad, M., Chadwick, A., Krawczyk, C., Ziegler, P., et al. (2010). In J. C. Doornenbal & A. G. Stevenson (Eds.), *Crustal structure and structural framework, in: Petroleum geological atlas of the southern Permian Basin area* (pp. 11–23). Houten, The Netherlands: EAGE Publications.

Hartog, A., Frignet, B., Mackie, D., & Clark, M. (2014). Vertical seismic optical profiling on wireline logging cable. *Geophysical Prospecting*, *62*(4), 693–701. doi:10.1111/1365-2478.12141

Henninges, J., Baumann, G., Brandt, W., Cunow, C., Poser, M., Schrötter, J., & Huenges, E. (2011). *A novel hybrid wireline logging system for downhole monitoring of fluid injection and production in deep reservoirs [Conference Proceedings]*. Paper presented at the 73rd EAGE Conference & Exhibition. Retrieved from doi:10.3997/2214-4609.20149727

Henninges, J., Martuganova, E., Stiller, M., Norden, B., & Krawczyk, C. M. (2021). Wireline distributed acoustic sensing allows 4.2 km deep vertical seismic profiling of the Rotliegend 150°c geothermal reservoir in the North German Basin. *Solid Earth*, *12*(2), 521–537. doi:10.5194/se-12-521-2021

Holl, H. G., Moeck, I., & Schandelmeier, H. (2005). *Characterization of the tectonosedimentary evolution of a geothermal reservoir—implications for exploitation (Southern Permian Basin, NE Germany)*. Paper presented at the World Geothermal Congress. Retrieved from https://www.geothermal-energy.org/pdf/IGAstandard/WGC/2005/0614.pdf

Jacquey, A. B., Cacace, M., Blöcher, G., Watanabe, N., Huenges, E., & Scheck-Wenderoth, M. (2016). Thermo-poroelastic

numerical modelling for enhanced geothermal system performance: case study of the Groß Schönebeck reservoir. *Tectonophysics*, *684*, 119–130. doi:10.1016/j.tecto.2015.12.020

Kästner, F., Giese, R., Planke, S., Millett, J. M., & Flóvenz, Ó. G. (2020). Seismic imaging in the Krafla high-temperature geothermal field, NE Iceland, using zero- and far-offset vertical seismic profiling (VSP) data. *Journal of Volcanology and Geothermal Research*, *391*, 106315. doi:10.1016/j.jvolgeores.2018.02.016

Krawczyk, C. M., Stiller, M., Bauer, K., Norden, B., Henninges, J., Ivanova, A., & Huenges, E. (2019). 3-D seismic exploration across the deep geothermal research platform Groß Schönebeck north of Berlin/Germany. *Geothermal Energy*, *7*(1), 15. doi:10.1186/s40517-019-0131-x

Lindsey, N. J., Rademacher, H., & Ajo-Franklin, J. B. (2020). On the broadband instrument response of fiber-optic DAS arrays. *Journal of Geophysical Research: Solid Earth*, *125* (2), e2019JB018145. doi:10.1029/2019JB018145

Lipus, M. P., Schölderle, F., Reinsch, T., Wollin, C., Krawczyk, C., Pfrang, D., & Zosseder, K. (2022). Dynamic motion monitoring of a 3.6 km long steel rod in a borehole during cold-water injection with distributed fiber-optic sensing. *Solid Earth*, *13*(1), 161–176. doi:10.5194/se-13-161-2022

Martuganova, E., Stiller, M., Bauer, K., Henninges, J., & Krawczyk, C. M. (2021). Cable reverberations during wireline distributed acoustic sensing measurements: their nature and methods for elimination. *Geophysical Prospecting*, *69*(5), 1034–1054. doi:10.1111/1365-2478.13090

Martuganova, E., Stiller, M., Norden, B., Henninges, J., & Krawczyk, C. M. (2022a). 3D deep geothermal reservoir imaging with wireline distributed acoustic sensing in two boreholes. *Solid Earth*, *13*(8), 1291–1307. doi:10.5194/se-13-1291-2022

Martuganova, E., Stiller, M. N., Henninges, B., & Krawczyk, C. M. (2022b). *3D DAS-VSP Data from the Groß Schönebeck Site, Germany, February 2017*. GFZ Data Services. doi:10.5880/GFZ.4.8.2022.014

Norden, B., Bauer, K., & Krawczyk, C. M. (2022). *Input and resulting structural and parameterized subsurface data for a geological model of the geothermal research platform Groß Schönebeck (North German Basin)*. GFZ Data Services. doi:10.5880/GFZ.4.8.2022.013

Norden, B., Bauer, K., & Krawczyk, C. M. (2023). From pilot knowledge via integrated reservoir characterization to utilization perspectives of deep geothermal reservoirs: the 3D Model of Groß Schönebeck (North German Basin). *Geothermal Energy*, *11*(1), 1. doi:10.1186/s40517-022-00242-2

Olasolo, P., Juárez, M., Morales, M., D'Amico, S., & Liarte, I. (2016). Enhanced geothermal systems (EGS): a review. *Renewable and Sustainable Energy Reviews*, *56*, 133–144. doi:10.1016/j.rser.2015.11.031

Regenspurg, S., Feldbusch, E., Byrne, J., Deon, F., Driba, D. L., Henninges, J., et al. (2015). Mineral precipitation during production of geothermal fluid from a Permian Rotliegend reservoir. *Geothermics*, *54*, 122–135. doi:10.1016/j.geothermics.2015.01.003

Roadmap for deep geothermal energy for Germany. (2022). Retrieved from doi:10.24406/publica-248

Schölderle, F., Lipus, M., Pfrang, D., Reinsch, T., Haberer, S., Einsiedl, F., & Zosseder, K. (2021). Monitoring cold water injections for reservoir characterization using a permanent fiber optic installation in a geothermal production well in the Southern German Molasse Basin. *Geothermal Energy*, *9*(1), 21. doi:10.1186/s40517-021-00204-0

Stiller, M., Krawczyk, C. M., Bauer, K., Henninges, J., Norden, B., Huenges, E., & Spalek, A. (2018). 3D Seismik am Geothermiestandort Groß Schönebeck. *BBR - Fachmagazin für Brunnen- und Leitungsbau*, *1*, 84–91. ((last access: 1 April 2022))

Suchi, E., Dittmann, J., Knopf, S., Müller, C., & Schulz, R. (2014). *Geothermieatlas zur darstellung möglicher nutzungskonkurrenzen zwischen CO2-Einlagerung (CCS) und tiefer geothermie in Deutschland*. Retrieved from https://www.geotis.de/homepage/sitecontent/info/publication_data/final_reports/final_reports_data/Endbericht_Geothermie_Atlas.pdf

Sun, Y., Li, H., Fan, C., Yan, B., Chen, J., Yan, Z., & Sun, Q. (2022). Review of a specialty fiber for distributed acoustic sensing technology. *Photonics*, *9*(5). doi:10.3390/photonics9050277

Tester, J., Anderson, B., Batchelor, A., Blackwell, D., DiPippo, R., Drake, E., et al. (2006). *The future of geothermal energy: impact of enhanced geothermal systems (EGS) on the United States in the 21st century* (Technical Report No. 0-615-13438-6). Massachusetts Institute of Technology.

Waagaard, O. H., Rønnekleiv, E., Haukanes, A., Stabo-Eeg, F., Thingbø, D., Forbord, S., et al. (2021). Real-time low noise distributed acoustic sensing in 171 km low loss fiber. *OSA Continuum*, *4*(2), 688–701. doi:10.1364/OSAC.408761

Weber, J., Born, H., Pester, S., Schifflechner, C., & Moeck, I. (2022). *Geothermal energy use in Germany, country update 2019–2021*. Paper presented at the European Geothermal Congress 2022. doi:10.24406/publica-592

Yu, G., Cai, Z., Chen, Y., Wang, X., Zhang, Q., Li, Y., et al. (2016). Walkaway VSP using multimode optical fibers in a hybrid wireline. *The Leading Edge*, *35*(7), 615–619. doi:10.1190/tle35070615.1

Zimmermann, G., Blöcher, G., Reinicke, A., & Brandt, W. (2011). Rock specific hydraulic fracturing and matrix acidizing to enhance a geothermal system — concepts and field results. *Tectonophysics*, *503*(1), 146–154. doi:10.1016/j.tecto.2010.09.026

Zimmermann, G., Moeck, I., & Blöcher, G. (2010). Cyclic waterfrac stimulation to develop an enhanced geothermal system (EGS)—conceptual design and experimental results. *Geothermics*, *39*(1), 59–69. Retrieved from doi:10.1016/j.geothermics.2009.10.003